

SiC multilayer photonic structures:

A new active filter design

Manuela Vieira

Electronics Telecommunication and Computer Dept.
ISEL . CTS-UNINOVA, DEE-FCT-UNL,
Lisbon, Portugal.
mv@isel.ipl.pt

Manuel Vieira

Electronics Telecommunication and Computer Dept.
ISEL . CTS-UNINOVA,
Lisbon, Portugal.
mvieira@deetc.isel.ipl.pt

Paula Louro

Electronics Telecommunication and Computer Dept.
ISEL . CTS-UNINOVA,
Lisbon, Portugal.
plouro@deetc.isel.ipl.pt

Alessandro Fantoni

Electronics Telecommunication and Computer Dept.
ISEL . CTS-UNINOVA,
Lisbon, Portugal.
afantoni@deetc.isel.ipl.pt

Vitor Silva

Electronics Telecommunication and Computer Dept.
ISEL . CTS-UNINOVA,
Lisbon, Portugal
vsilva@isel.pt.

Abstract— Stacked layered pin a-SiC/a-Si devices based on a filter design are approached from a reconfigurable point of view. This paper shows that a double SiC/Si pin photodiode can be de-composed into two photonic active filters changeable in function. Reconfiguration is provided by optical control signals to the optoelectronic front and back pin building blocks. Depending on the wavelength and irradiation side of the external optical bias the device acts either as a short- and a long- pass band filter or as a band-stop filter, amplifying or rejecting a specific wavelength range. Particular attention is given to the amplification coefficient weights, which allow taking into account the wavelength background effects. We illustrate these effects in detail and discuss the filters transfer function characteristics. We present examples of filters and we propose a reconfigurable device for directed optical logic. An algorithm to decode the information is presented. An optoelectronic model supports the optoelectronic logic architecture.

Keywords-Optical filters, Photonics, multilayer devices, integrated filters

I. INTRODUCTION

Multilayered structures based on amorphous silicon technology are expected to become reconfigurable to perform WDM optoelectronic logic functions and provide photonic functions such as signal amplification and switching [1, 2]. They will be a solution in WDM technique for information transmission and decoding in the visible range [3]. The basic operating principle is the exploitation of

the physical properties of a nonlinear element to perform a logic function, with the potential to be rapidly biasing tuned. Amplification and amplitude change are two key functionality properties outcome of a balanced interaction between frequency and wavelength of the optical signal and background wavelength and placement within a WDM link. Any change in any of these factors will result in filter readjustments. Here, signal variations with and without front and back backgrounds move electric field action up and down in a known time frame. A numerical simulation support new optoelectronic logic architecture.

II. DEVICE CONFIGURATION AND OPERATION

The active device consists of a p-i'(a-SiC:H)-n/p-i(a-Si:H)-n heterostructure with low conductivity doped layers (Fig.1). The thicknesses and optical gap of the front i' (200 nm; 2.1 eV) and back i- (1000 nm; 1.8 eV) layers are optimized for light absorption in the blue and red ranges, respectively. Several monochromatic pulsed lights, separately ($\lambda_{R,G,B}$ input channels) or in a polychromatic mixture (multiplexed signal), at different bit rates illuminated the device from the glass side. Steady state optical bias with different wavelength are superimposed (400nm-800 nm) from the front or from the back sides and the generated photocurrent measured at -8 V. The device operates within the visible range using as input color channels (data) the wave square modulated light (external regulation of frequency and intensity) supplied by a red (R: 626 nm; 51 $\mu\text{W}/\text{cm}^2$), a green (G: 524 nm; 73 $\mu\text{W}/\text{cm}^2$) and a blue (B:

470 nm; 115 $\mu\text{W}/\text{cm}^2$) LED. Additionally, steady state red, green, blue and violet (background) was superimposed by LEDs driven at a constant current value (R: 625 $\mu\text{W}/\text{cm}^2$, G: 515 $\mu\text{W}/\text{cm}^2$, B: 680 $\mu\text{W}/\text{cm}^2$, V: 2800 $\mu\text{W}/\text{cm}^2$).

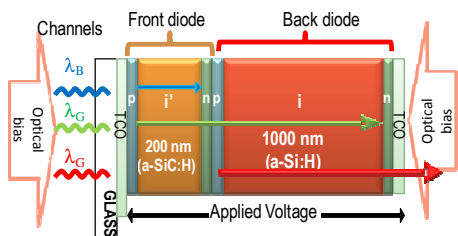


Figure 1. Device design and operation.

III. TRANSFER FUNCTION CHARACTERISTICS

The transfer function magnitude (or gain) allows to determine the ability of the optical filter to distinguish between signals at different wavelengths. The spectral sensitivity was tested through spectral response measurements under different frequencies, with and without steady state optical bias applied either from the front or back side (Fig.1).

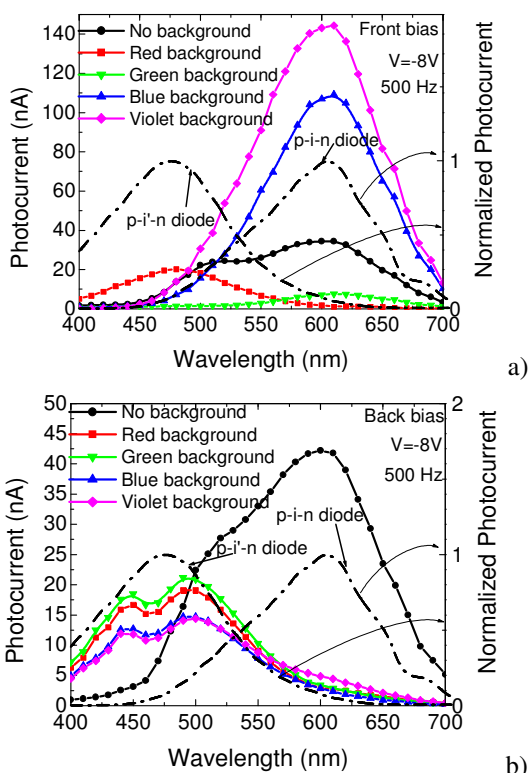


Figure 2. Photocurrent without and with front (a) and back (b) backgrounds. The current of the individual photodiodes are superimposed (dash lines).

In Fig. 2, at 500 Hz, the spectral photocurrent (symbols) is displayed under red, green, blue and violet background and without it. In Fig. 2a the steady state optical bias was applied from the front side and in Fig. 2b from the back side. For comparison the normalized spectral photocurrent for the front, p-i'-n, and the back, p-i-n, photodiodes (dash lines) are superimposed.

Experimental data shows that the front and back building blocks, separately, presents the typical response of single p-i-n cells with intrinsic layers based on a-SiC:H or a-Si:H materials, respectively. The front diode cuts the wavelengths higher than 550 nm while the back one rejects the ones lower than 500 nm. The overall device presents an enlarged sensitivity when compared with the individual ones. Results show that under front irradiation the sensitivity is much higher than under back irradiation. Under front irradiation (Fig.2a) the violet background amplifies the spectral sensitivity in the visible range while the blue optical bias only enhances the spectral sensitivity in the long wavelength range (>550 nm) and quenches it in the others. Under red bias, the photocurrent is strongly enhanced at short wavelengths and disappears for wavelengths higher than 550 nm. Under green the sensitivity is strongly reduced in all the visible spectra. In Fig. 2b, whatever the wavelength of the backgrounds, the back irradiation strongly quenches the sensitivity in the long wavelength range (> 550nm) and enhances the short wavelength range. So, back irradiation, tunes the front diode while front irradiation, depending on the wavelength used, tunes the back one.

IV. OPTICAL BIAS AMPLIFICATION

In Fig. 3 the spectral gain, defined as the ratio between the spectral photocurrents under red (α^R), green (α^G) blue (α^B) and Violet (α^V) illumination and without it is plotted at 500 Hz and 3500 Hz. The optical bias is applied from the front side, in Fig. 3a and from the back side, in Fig. 3b.

Under front bias and red irradiation the gain is high at short wavelengths and strongly lowers for wavelengths higher than 550 nm, acting as a short-pass filter. Under green background and high frequencies, the device behaves as a band-stop filter that screens out the medium wavelength range (green) enhancing only the photocurrent for wavelengths outside of that range. Under blue and violet light the devices works as a long-pass filter for wavelengths higher than 550 nm, blocking the shorter wavelengths. Back light, whatever the frequency, leads to a short-pass filter performance. Experimental results show that by combining the background wavelengths and the irradiation side the short-, medium- and long- spectral region can be sequentially tuned.

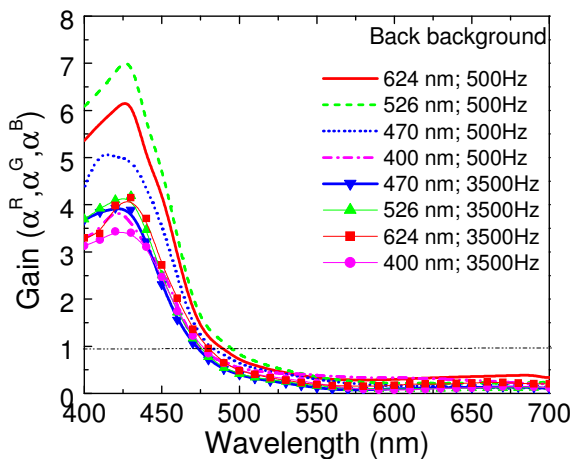
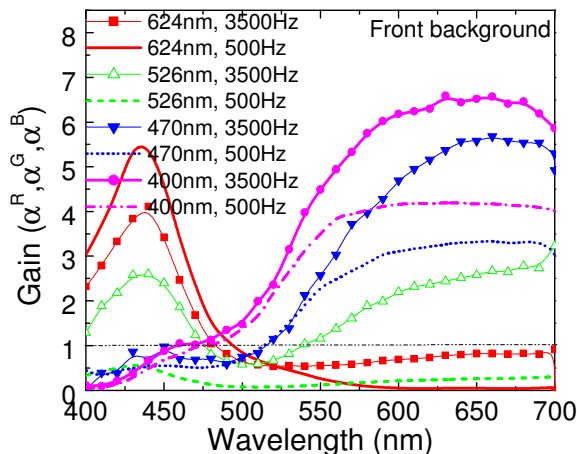


Figure 3. Spectral gain under red (α_R), green (α_G), and blue (α_B) optical bias, applied from the front (a) and the back (b) sides at different frequencies.

In Fig. 4 the front and back gains as a function of the frequency, at fixed wavelengths: 470 nm (blue channel), 526 nm (green channel) and as 624 nm (red channel) is plotted under 400 nm applied optical bias from the front (symbols) and back (lines) sides. Results show that, no matter what the irradiation side, the blue and green channel gain does not depend on the frequencies, while the red one increases under front illumination and is strongly reduced under back light. In Fig. 5 under front and back violet irradiation, it is displayed the spectral gain for three different frequencies.

Results show that, whatever the frequency, the device acts as an active long-pass filter under front irradiation and a low-pass filter under back irradiation. Under front bias the gain is higher than the unity for wavelengths above 500nm resulting in an amplification of the green and red spectral ranges. Back irradiation only amplifies the short wavelength range and extinguishes the others.

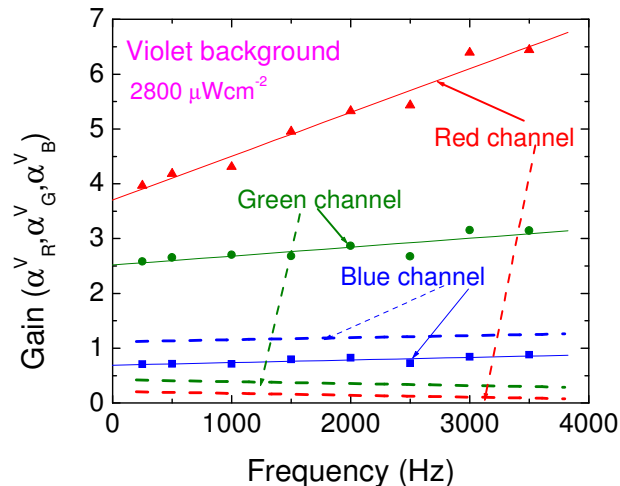


Figure 4. Input front (symbols) and back (lines) channel gains (α_R , α_G , α_B), as a function of the frequency.

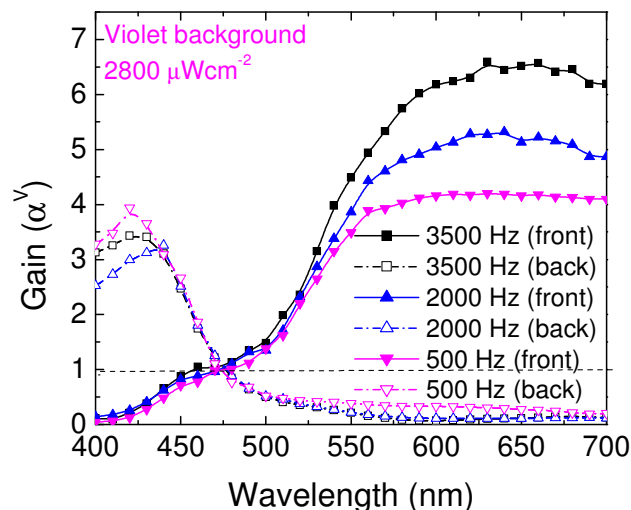


Figure 5. Spectral gain under violet optical bias (α^V) for different frequencies.

V. ENCODER AND DECODER DEVICE

To analyze the device under information-modulated wave and uniform irradiation, three monochromatic pulsed lights separately (red, green and blue input channels, Fig. 6a) or combined (multiplexed signal, Fig. 6b) illuminated the device at 6000 bps. Steady state violet optical bias was superimposed separately from the front (solid lines, pin_1) and the back (dash lines, pin_2) sides and the photocurrent generated measured at -8 V. The transient signals were normalized to their values without background. In Fig. 6b the multiplexed signal without and with background are displayed (solid lines). Here the input channels without optical bias (dash lines) are also superimposed. On the top of the figure the signals used to drive the input channels are shown.

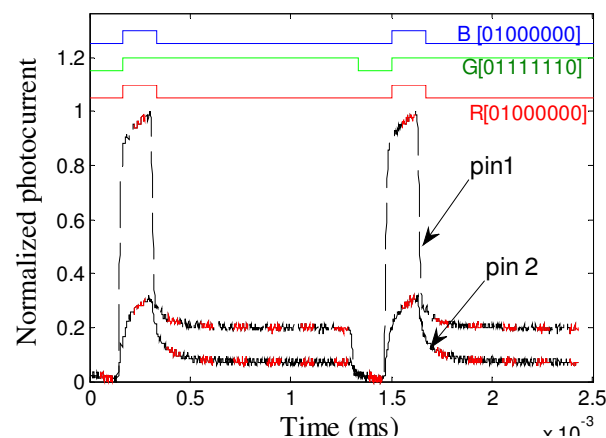
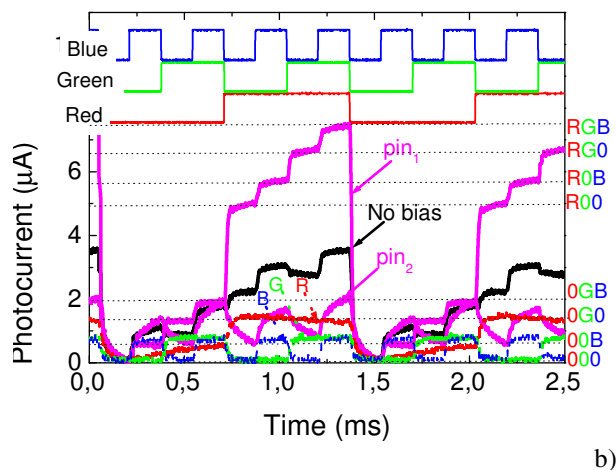
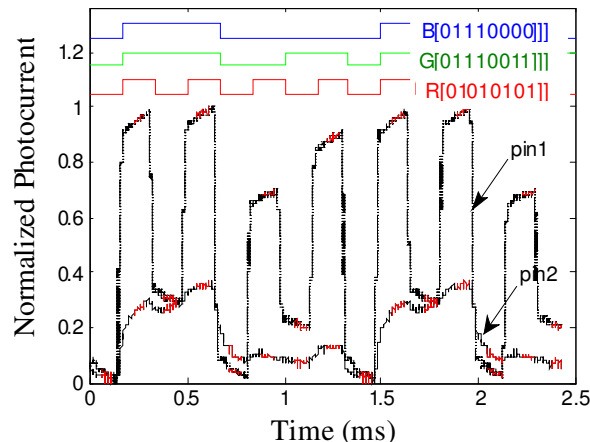
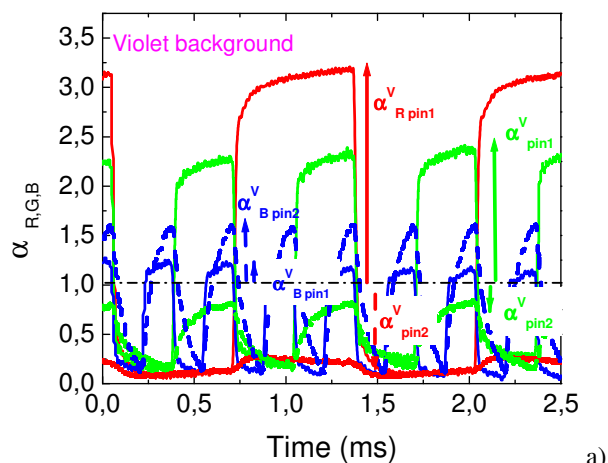


Figure 6. a) Normalized red, green and blue transient signals at -8V with violet (400 nm) steady state optical bias applied from the front side (apin1) and from the back side (apin2). b) Input R,G,B channels and multiplexed output without (no bias) and under front (pin1) and back (pin2) irradiation.

Figure 7. MUX signal under front and back irradiation. On the top the DEMUX signals obtained using the decoder algorithm is displayed as well as the binary bit sequences.

Even under transient conditions, as in Fig 3, the front background presents the same nonlinear dependence on the wavelength. It enhances mainly the light-to-dark sensitivity in the medium-long wavelength ranges. Violet radiation is absorbed at the top of the front diode, increasing the electric field at the least absorbing cell [4], the back diode, where the red and part of the green channels generate optical carriers. So the collection is strongly enhanced ($\alpha_{Gpin1}^V=2.2$, $\alpha_{Rpin1}^V=3.1$) while the blue collection stays near its dark value ($\alpha_{Bpin1}^V=1.1$).

Under back irradiation the small absorption depth of the violet photons across the back diode quenches the electric field and so, the red collection almost disappears ($\alpha_{Rpin2}^V=0.2$). Blue channel is absorbed across the front diode where the electric field is enhanced resulting in an increase collection of the blue channel ($\alpha_{Bpin1}^V=1.6$).

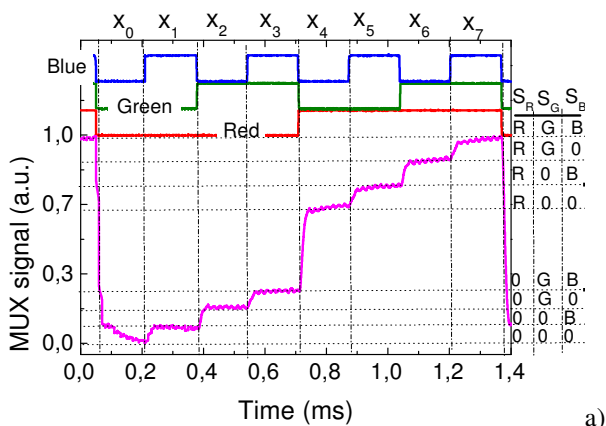
Since the green channel is absorbed across front and back diodes its collection is balanced by the increased collection in the front diode and its reduction at the back one ($\alpha_{Gpin2}^V=0.7$). Under front irradiation, the encoded multiplexed signal presents eight separate levels (2^3) each one related with an RGB bit sequence (right side of the Fig. 6b). Those levels can be grouped into two main classes due to the high amplification of the red channel under front irradiation. The upper four levels are ascribed to the presence of the red channel ON and the lower four to its absence allowing the red channel decoder. Since under front irradiation the green channel is amplified, the two highest levels, in both classes, are ascribed to the presence of the green channel and the two lower ones to its lack. Under back irradiation, the red channel is suppressed, the blue enhanced and the green reduced, so the encoded multiplexed signal presents only four main separate levels (2^2). The two higher levels correspond to the presence of the blue channel ON with or without the green ON respectively, and the other two to its absence. The blue channel is then decoded. We have used this simple algorithm to decode the multiplex signal.

The results are displayed in Fig. 7 for two different bit sequences. An excellent fit was obtained.

Results show that the pinpi'n multilayered structure become reconfigurable under front and back irradiation. They perform WDM optoelectronic logic functions providing photonic functions such as signal amplification, filtering and switching. So, by means of optical control applied to the front or back diodes, the photonic function is modified from a long- to a short-pass filter, giving a step reconfiguration of the device.

VI. PHOTONIC ACTIVE FILTERS

In the pi'n/pin device the morphology of filter system results from the interaction of the electric field under applied optical bias (red, green, blue, violet) and the transient electric field induced by the input channels. This interaction results in electric field lines that guides the photocarriers generated by the input channels. The flow rate of the optical carriers through those field lines towards the output depends on the on/off state of the color channels.



MUX
↔
DEMUX

Inputs								Outputs			
x_0	x_1	x_2	x_3	x_4	x_5	x_6	x_7	S_2	S_1	S_0	γ
0	0	0	0	0	0	0	1	1	1	1	■
0	0	0	0	0	0	1	0	1	1	0	■
0	0	0	0	0	1	0	0	1	0	1	■
0	0	0	0	1	0	0	0	1	0	0	■
0	0	0	1	0	0	0	0	0	1	1	□
0	0	1	0	0	0	0	0	0	1	0	□
0	1	0	0	0	0	0	0	0	0	1	□
0	0	0	0	0	0	0	0	0	0	0	□

Figure 8. MUX signal outputs (a) and truth table (b) of the encoders that perform 8-to-1 multiplexer (MUX) function, under front violet irradiations.

In Fig. 8a an output MUX signal under front violet irradiation is displayed. On the top the signals used to drive the input channels are displayed showing the presence of all the possible 2^3 on/off states ($x_0...x_7$). Fig. 8b shows the truth table of an encoder that performs 8-to-1 multiplexer (MUX) function. In the inputs ($x_0...x_7$) the index of each bit is related with of the first (highest) nonzero logic input. To understand this mapping, in Fig. 8b, for the input x_7 and output S_2 , the first nonzero logic input is $7(2^2+2^1+2^0)$, which corresponds an output [111]. That OR gate is expressed as $S_2=x_7+x_6+x_5+x_4$. Under front violet irradiation, $\alpha^V_R \gg 1$, $\alpha^V_G > 1$ and $\alpha^V_B \sim 1$ (Fig. 5). So, the correspondence between the outputs S_2, S_1, S_0 and the on/off state of the input channels, S_R, S_G, S_B , is obvious.

The DEMUX, on the other hand, sends the input logic signal to one of its eight outputs ($y_s = x$), according to the optoelectronic demux algorithm.

To convert from a particular logic function (8-to-1 MUX) to another (FILTER), one needs only to redefine the input and output signals and to reconfigure the operation mode. Taking into account Fig. 5a, under back violet bias control, a step change in configuration occurs. Here, the encoded four level signal is grouped in two classes, the uppers two levels, where the blue channel is ON and the others where it is OFF (4-to-1 multiplexer; short-pass filter function).

VII. OPTOELECTRONIC MODEL

Based on the experimental results and device configuration an optoelectronic model, made out of a short-pass and a long-pass filter (see Fig. 4 and Fig. 5) and supported by the complete dynamical large signal Ebers-Moll model, was developed [5, 6]. The equivalent circuit, made out of a short-pass filter (front phototransistor, Q_1) and a long-pass filter (back phototransistor, Q_2) sections connected in parallel is displayed in Fig. 9a. The charge stored in the space-charge layers is modeled by the capacitor C_1 and C_2 . R_1 and R_2 model the dynamical resistances of the internal and back junctions under different dc bias conditions. To allow independent blue, red and green channels transmission four square-wave current sources with different intensities are used; two of them, $\alpha_1 I_B$ and $\alpha_2 I_R$, with different frequencies to simulate the input blue and red channels and the other two, $\alpha_1 I_{Gpin}$ and $\alpha_2 I_{Gpin}$, with the same frequency but different intensities, to simulate the green channel due to its asymmetrical absorption across both front and back phototransistors.

When the pi'n/pin device is reverse-biased, the base-emitter junction of both transistors are inversely polarized and conceived as phototransistors, taking, so, advantage of the amplifier action of adjacent collector junctions which are polarized directly. This results in a current gain proportional to the ratio between both collector currents. The amplifying elements, α_1 and α_2 , can provide gain if needed and attenuate unwanted wavelengths (<1) while amplifying (>1) desired ones. The values and the strategic placement of the resistors determine the basic shape of the output signals. So, the flow of current through the resistor connecting the two transistor bases, R_1 , is proportional to the difference in the voltages

across both capacitors (charge storage buckets). The device is formed by two reconfigurable building-blocks (the front and the back diodes) interconnected both optical and electrically, each of which has a distinct function. Depending on the side and wavelength of the optical bias control, the magnitude of the *signals* are changed by an α factor, and so the voltages across the front and the back or both photodiodes. The device behaves like an optoelectronic controlled transmission system that stores, amplifies and transports the minority carriers generated by the current pulses, through capacitors C_1 and C_2 .

To validate the model under front and back irradiation, in Fig. 9b, the experimental (solid lines) and the simulated (symbols) waveform under negative bias and violet front and back backgrounds is shown. The bit sequences to drive the channels are shown in the top of the figure to guide the eyes. To simulate the violet background, the current sources intensities that model the input channels (individual channels, Fig. 6b) were multiplied by the on/off ratio between the input channels with and without optical bias ($\alpha_{R,G,B}^{V_{pin1,2}}$, Fig. 6a). A good agreement between experimental and simulated data was achieved.

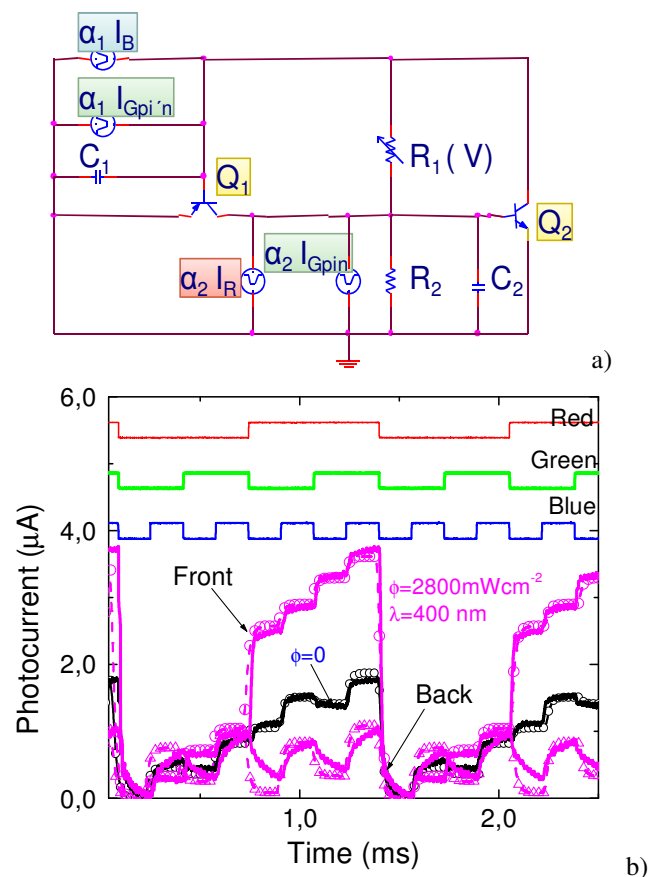


Figure 9. Simulated (symbols) and experimental (solid lines) multiplex signals under front and back violet background.

The device is formed by two reconfigurable building-blocks (the front and the back diodes) interconnected both optical and electrically, each of which has a distinct function. Depending on the side and wavelength of the optical bias control, the magnitude of the *signals* are changed by an α factor, and so the voltages across the front and the back or both photodiodes. Under front irradiation the expected optical amplification in the short wavelength range and quenching in the long ones is observed due to the effect of the active multiple-feedback filter when the back diode is light triggered. The opposite occurs under back irradiation.

VIII. CONCLUSIONS

Combined tunable converters based on SiC multilayer photonics active filters are analyzed. Results show that the light-activated pi'n/pin a-SiC:H devices combine the demultiplexing operation with the simultaneous photodetection and self amplification of an optical signal. The output waveform presents a nonlinear amplitude-dependent response to the wavelengths of the input channels. Depending on the wavelength of the external background it acts either as a short- or a long- pass band filter or as a band-stop filter. A two stage active circuit is presented and gives insight into the physics of the device.

ACKNOWLEDGMENT

This work was supported by FCT (CTS multi annual funding) through the PIDDAC Program funds and PTDC/EEA-ELC/111854/2009 and PTDC/EEA-ELC/120539/2010.

REFERENCES

- [1] C. Petit, M. Blaser, Workshop on Optical Components for Broadband Communication, ed. by Pierre-Yves Fonjallaz, Thomas P. Pearsall, Proc. of SPIE Vol. 6350, 63500I, (2006).
- [2] S. Ibrahim, L. W. Luo, S. S. Djordjevic, C. B. Poitras, I. Zhou, N. K. Fontaine, B. Guan, Z. Ding, K. Okamoto, M. Lipson, and S. J. B. Yoo, paper OWJ5. Optical Fiber Communications Conference, OSA/OFC/NFOEC, San Diego, 21 Mar 2010.
- [3] S. Randel, A.M.J. Koonen, S.C.J. Lee, F. Breyer, M. Garcia Larrode, J. Yang, A. Ng'Oma, G.J Rijckenberg, and H.P.A. Boom. " ECOC 07 (Th 4.1.4). (pp. 1-4). Berlin, Germany, 2007.
- [4] M. Vieira, A. Fantoni, P. Louro, M. Fernandes, R. Schwarz, G. Lavareda, and C. N. Carvalho, Vacuum, 82, Issue 12, 8 August 2008, pp: 1512-1516.
- [5] M A Vieira, M. Vieira, M. Fernandes, A. Fantoni, P. Louro, M. Barata, Thin-Film Silicon Science and Technology — 2009, MRS Proceedings Volume 1153, A08-03.
- [6] M. A. Vieira, M. Vieira, J. Costa, P. Louro, M. Fernandes, A. Fantoni, Sensors & Transducers Journal, 9, Special Issue, December 2010, pp.96-120.